SYNTHESIS, CHARACTERIZATION AND EVALUATION OF Ag-TiO$_2$ NANOCOMPOSITES FOR PHOTO-CATALYTIC DEGRADATION OF SELECTED CHLOROPHENOLS

K. KOTLHAO, F. M. MTUNZI, V. PAKADE, I. P. EJIDIKE, M. J. KLINK[*]
Vaal University of Technology, Andries Potgieter Boulevard, Vanderbijlpark, 1911, South Africa

Anatase TiO$_2$ and Ag nanoparticles were synthesized using reduction and precipitation method respectively. The prepared nanoparticles and nanocomposites were characterized using ultraviolet visible spectroscopy (UV-Vis) photoluminescence (PL), X-ray diffractometry (XRD), scanning transmission electron spectroscopy (STEM) and Energy Dispersive X-ray (EDX). The prepared nanoparticles (Ag, TiO$_2$) and nanocomposites (Ag-TiO$_2$: 1, 3, 5 %) were investigated for their photocatalytic properties on 2-chlorophenol, 2,4- dichlorophenol and 2,4,6-trichlorophenol using UV light for irradiation. The UV results showed band gap reduction from 3.38 (TiO$_2$), 3.36 (Ag-TiO$_2$ 1 %), 3.32 (Ag-TiO$_2$ 3 %) to 2.99 (Ag-TiO$_2$ 5%). The UV-Vis spectrum for pure silver showed a slightly broad absorbance peak in the range 384 - 410 nm which is characteristic of surface plasmon resonance for silver. The XRD pattern obtained corresponded to the anatase phase according to JCPDS card no. 21-1272. The estimated crystallite sizes ranged from 9.40 nm, 12.41 and 11.44 nm for Ag-TiO$_2$ (1 %) Ag-TiO$_2$ (3 %) and Ag-TiO$_2$ (5 %) respectively. The STEM images did not show the expected trend in size, however, the presence of silver appeared as bright white irregular shaped spots. The mean particle size ranged from about 6.78 ±1.44 nm, 10.64 ± 1.91 nm, and 8.54 ± 2.01 for Ag-TiO$_2$ (1 %) Ag-TiO$_2$ (3 %) and Ag-TiO$_2$ (5 %) respectively. Photocatalytic degradation showed better performance with Ag- TiO$_2$ at initial concentration of 5 ppm and pH 11 compared to bare Ag and TiO$_2$.

1. Introduction

Nanosized TiO$_2$ has received great attention in research due to its desirable properties such as high surface area to volume ratio [1], chemical reactivity as well as photocatalytic activity. TiO$_2$ exists in three crystalline phases: brookite, rutile and anatase. Methods of synthesizing the anatase phase are of interest to this study due to its superiority in photo-catalytic properties [2, 3]. There are several methods for preparing TiO$_2$ these include among others microwave assisted [4], acid treatment [5] and sol-gel [2, 3, 6]. The wet chemical methods such as sol-gel are preferred for anatase phase nanoparticles because they allow for control of reaction conditions. However, the photocatalytic activity of TiO$_2$ is relatively limited due to the fast recombination of the photo excited electron with the photo generated holes [7]. One way of enhancing the photocatalytic activity is by combining the catalyst with another semiconductor or metal capable of producing "charge separation effect'' [6]. Metals such as Au, Pt and Ag can effectively act as electron scavengers in the presence of a catalyst to increase its photocatalytic properties [7]. Silver can enhance the photocatalytic properties of the catalyst and also possesses antibacterial activity [8]. This has led to the recent research activities on Ag doped TiO$_2$ [1, 7, 9] and Ag doped ZnO [10-11].

[*] Corresponding author: michaelk1@vut.ac.za

The photocatalytic property is influenced by the morphology of the nanomaterials, which is a result of the conditions applied during the synthesis stage. Examples of these in wet chemical methods are calcination temperatures, use of capping agents, reaction time, precursor concentration and type etc. For this reason, the methods of nanoparticles synthesis continue to be explored for different applications.

Precipitation [12] and sol- gel methods [13-14] were employed in three studies using titanium tetrabutoxide (TBT) as a precursor. The annealing temperatures were 450-650°C, 230°C and 450°C respectively. The nanoparticles produced in both were spherically shaped with sizes ranging from 18-22 nm, 8-16 nm and 5-13 nm respectively and were all in the anatase phase. It is therefore convincing that TBT is capable of readily producing small sized nanoparticles of the desired anatase phase for photocatalytic degradation, even without the use of a surfactant [2, 3]. On the hand silver nanoparticles have been prepared using silver nitrate with either a citrate [15], borohydride [15] as a reducing agent. It has been found that borohydride produces nanoparticles that are more mono dispersed compared to citrate. However, the reduction method is normally associated with agglomeration with both reducing agents, hence the need to use surfactants [16].

In this study, Ag and TiO$_2$ nanoparticles were synthesized using reduction, and precipitation methods with TBT as a precursor. We further synthesized Ag-TiO$_2$ nanocomposites using a combination of the reduction and precipitation methods. The amount of Ag was varied as 1, 3 and 5 wt %. Polyvinlylpyrrolidone (PVP) was added to prevent agglomeration. Compared to sodium dodecylsulphate (SDS) and Hexadecyltrimethylammonium bromide (CTAB), nanoparticles in the presence of PVP have been found to be relatively less agglomerated [17]. Due to the fact that the shape and size of nanoparticles are influenced by several factors in the synthesis method. The shape and size also have a bearing on the effectiveness of the photocatalytic activity of catalyst, we find that different approaches for nanoparticle synthesis will continue to be explored. The prepared nanoparticles were characterized using ultraviolet–visible spectroscopy (UV-Vis), photoluminescence (PL), X-ray diffractometry (XRD), scanning transmission electron microscopy (STEM) and energy dispersive X-ray spectroscopy (EDX). The nanoparticles and nanocomposites were further investigated for their efficiency to degrade 2-chlorophenol, 2,4-dichlorophenol and 2,4,6-trichlorophenol at two initial concentrations (25 ppm 5 ppm) and pHs 6.0, 8.0 and 11.0. The catalytic degradation performance of Ag-TiO$_2$ on chlorophenols (with different amounts of Ag; 1, 3 and 5 %) was compared to that of pure Ag and TiO$_2$ under UV light.

2. Experimental details

2.1 Materials details/chemical details

All the chemicals used for synthesis were used without any further purification. Titanium tetrabutoxide, acetic acid, ethanol, sodium borohydride, silver nitrate and PVP were purchased from Sigma Aldrich, South Africa.

2.2 Preparation of TiO$_2$ nanoparticles

A 50 ml ethanolic solution of 7,74ml titanium tetrabutoxide (TBT) was placed in a beaker and 50ml of 10.32 ml acetic acid (AcOH) added slowly, drop by drop under constant stirring at 4000rpm. Immediately, 0.9 g of polyvinlylpyrrolidone (PVP) dissolved in 10 ml of ethanol was added to prevent agglomeration. The mixture continued under stirring for a further 30 minutes after addition of PVP. The mixture formed a white precipitate as an indication of the formation of titanium hydroxide. The mixture was removed from the magnetic stirrer, covered with a parafilm and allowed to maturate for 12 hours. The precipitate was centrifuged at 2000rpm for 10 minutes, washed with deionized water and ethanol then dried in an oven at 80°C. The prepared powder was calcined at 500°C for 2 hours to convert titanium hydroxide to TiO$_2$ nanoparticles [18]. The proposed reaction is shown in equations (1-3) [19].

Hydrolysis:

$$Ti(OC_4H_9)_4 + 4H_2O \rightarrow Ti(OH)_4 + 4C_4H_9OH \qquad (1)$$

Poly-condensation:

$$Ti(OH)_4 \rightarrow TiO_2 \text{ (precipitate)} + H_2O \qquad (2)$$

Calcining:

$$TiO_2 \text{ (precipitate)} \rightarrow TiO_2 \qquad (3)$$
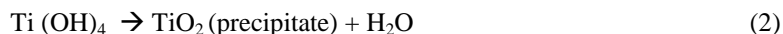
2.3 Preparation of Ag nanoparticles

An amount of 0.85 g and 0.23 g silver nitrate ($AgNO_3$) and sodium borohydride ($NaHB_4$) were each dissolved in 50 ml ethanol. The $NaHB_4$, a reducing agent, was slowly added into the solution of $AgNO_3$ under an ice bath and constantly stirred at 4000 rpm. Immediately, 0.9 g of PVP dissolved in 10ml of ethanol was added to prevent agglomeration. Stirring was continued for about 45 minutes. The beaker was covered with aluminum foil to avoid direct sunlight. A colourless solution turned yellowish as an indication of the formation of silver nanoparticles. The mixture was centrifuged at 2000 rpm for 10 minutes, washed with deionized water then dried at 80°C. The chemical reaction for the preparation of silver nanoparticles is represented by equation 4 [20-21].

$$2AgNO_3\,(aq) + 2NaBH_4\,(aq) \rightarrow 2Ag(s) + H_2\,(g) + B_2H_6 + 2NaNO_3\,(aq) \qquad (4)$$
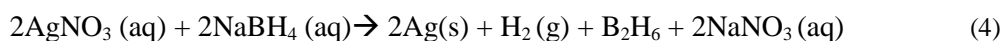
2.4 Preparation of Ag – TiO$_2$ nanocomposites

To prepare Ag-TiO$_2$ nanocomposites, the procedure for synthesis of TiO$_2$ was followed and within the first 30 minutes of stirring 0,077g of silver nitrate dissolved in 25 ml ethanol was slowly added. The reaction proceeded for 10 minutes then 0,010 g of sodium borohydride in 25 ml ethanol was added slowly to reduce the silver ions into silver atoms. Immediately, 10 ml ethanol solution of 0.9 g polyvinlylpyrrolidone (PVP) was added to prevent agglomeration. The mixture was stirred for a further 30 minutes. The light brown precipitate, in a beaker covered with aluminum foil was removed from the magnetic stirrer and allowed to maturate for 12 hours. The precipitate was centrifuged at 2000 rpm for 10 minutes and dried in an oven at 80°C. The prepared powder was calcined at 500 ^{o}C for 2 hours to convert titanium hydroxide to TiO$_2$ nanoparticles. The reaction was repeated with the amount of silver nitrate varied from 1, 3 and 5wt%.

2.5 Characterization

2.5.1 Ultra Violet –Visible

The optical properties of the Ag, TiO$_2$ and Ag-TiO$_2$ nanoparticles/nanocomposites were characterized using the Perkin Elmer UV-Vis, T80 double beam spectrophotometer. The absorption was carried out in the wavelength range from 200 to 900 nm.

2.5.2 Photoluminescence (PL)

Photoluminescence was used to study the electronic structure of the nanomaterials. The excitation wavelength was scanned from 200 to 600 nm.

2.5.3 XRD

The effect of Ag on crystalline structure of TiO$_2$ was investigated using Shimadzu-XRD 700, X-Ray Diffractometer, Cu Kα radiation (l = 1.154056 Å). Analysis was carried out in the 2Ө range from 10 – 90°.

2.5.4 STEM and EDX

STEM analysis was done at the University of Stellenbosch. South Africa.

2.5.5 Photodegradation

The photocatalytic activity of Ag, TiO$_2$, and Ag- TiO$_2$ (1, 3 and 5wt%) was studied by investigating the degradation of chlorophenols. The photocatalytic degradation experiments were performed in a batch mode using a photocatalytic reactor. The reactor was fitted with a water cylinder of 400 ml volume capacity. The photoreactor consisted of the 16 W UVC lamp. The

reactor was filled with 300 ml mixture of 25 and 5 ppm of 2-chlorophenol, 2,4-dichlorophenol and 2,4,6-trichlorophenol organic contaminants and nanoparticles/ nanocomposites. The pH was adjusted to pH 6.0, 80 and 11.00, using NaOH and HCl. The mixture was sonicated for 20 min for equilibration of the nanoparticles and the chlorophenols. The mixture was continuously bubbled using air from a peristaltic pump. For the first 30 min. the reaction was allowed take place without light to allow for adsorption of the nanoparticles onto the chlorophenols. The reaction was then monitored for further 120 minutes under UV light with aliquots of the mixture sampled through a 0.45µm filter membrane every 20 minutes [22-23]. The residual amount of the organic contaminants was determined using the T80 UV-Vis double beam spectrophotometer at λmax of 306.

3. Results and discussion

Fig. 1(a) show the UV-Vis absorption spectra, Tauc plots (b) and photoluminescence graph (c) for TiO_2 and Ag- TiO_2. Tauc plots were used to establish the band gap energies (Eg) of TiO_2 and Ag- TiO_2. This is a plot of $(\alpha h v)^2$ versus photon energy in (hv). The optical band gap energy, Eg was determined by extrapolating the linear portion to

$$(\alpha h v)^2 = 0 [26].$$

$$\alpha = K(h\upsilon - E_g)^2/h\upsilon \qquad (5)$$

where, K is constant, hv is the photon energy and Eg is the band gap energy for indirect transitions and (α), the absorption coefficient. The band gap of TiO_2 was 3.38, which was higher than 3.2 eV for the bulk. This showed a blue shift as a result of the particle size reduction [24]. Addition of silver atoms into the TiO_2 crystal structure showed a slight red shift towards a higher wavelength, between 1 and 3 wt, 3%, but an observable red shift at 5 wt % of Ag. The band gaps reduced from 3.38 (TiO_2), 3.36 (Ag-TiO_2 1 %), 3.32 (Ag-TiO_2 3wt %) to 2.99 (Ag-TiO_2 5wt %). This could contribute to an enhanced photocatalytic degradation [25]. The UV-Vis spectrum for pure silver showed a slightly broad absorbance peak in the range 384 - 410 nm which is characteristic of surface plasmon resonance for silver nanoparticles [26]. However, the absorption peak for silver was not observed in the Ag-TiO_2 (1- 5wt %) spectra. This could mean that the silver atoms were only distributed throughout the TiO_2 structure [27-29].
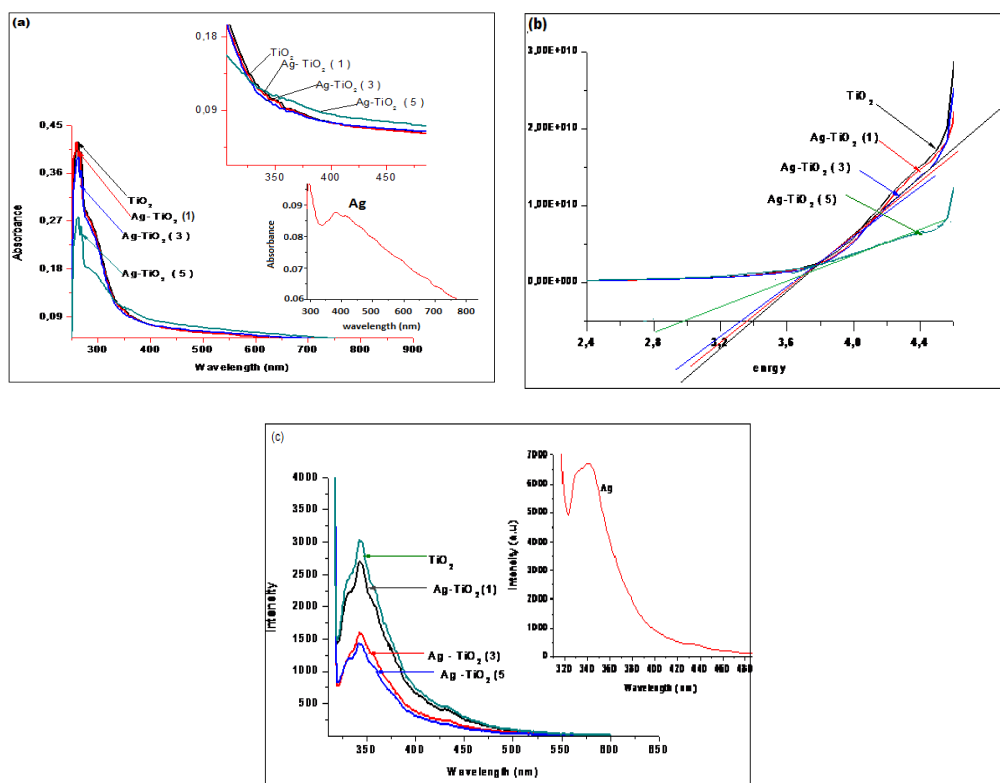
Fig. 1. UV-Vis absorption spectra (a), variation of (αhν)^2 against energy (Tauc plots) (b) for and photoluminescence spectra (c) of Ag, TiO$_2$ and Ag $_x$-TiO$_2$, (for x = 1, 3 and 5 %).

Photoluminescence spectroscopy (PL) is an optical non-destructive method for understanding the structure and properties of the active sites of a semiconductor. The PL emission signals of semiconductor materials result from the recombination of the photo generated electrons and holes. For a low PL intensity, the recombination rate is lower and photocatalytic activity is enhanced and vice versa [29]. Fig. 1 (c) shows the normalised PL emission spectra of TiO$_2$ and Ag-TiO$_2$ (at 1, 3 and 5 % of Ag) which was excited at 310 nm. As the Ag concentration was increased from 1, 3 and 5 wt % on there was a reduction in intensity. This was attributed to possible reduction in the recombination rate [29-30].

Fig. 2 shows the XRD pattern for TiO$_2$ and Ag-TiO$_2$. The diffraction peaks at 25,50^o, 37,89^o 48,40^o, 53,98^o, 55,29^o, 62,65^o, 68,47^o, 70,57^o, 75,34^o were indexed to (101), (004), (200), (105), (211), (204), (220), (220) and (215) crystalline planes respectively. This corresponded to the anatase phase of TiO$_2$ according to JCPDS Card No. (21-1272). The anatase phase of TiO$_2$ is preferred over rutile and brookite for photocatalytic degradation of organic compounds [31]. The Ag peaks could not be observed in all the Ag-TiO$_2$ (1, 3 and 5 wt %) XRD patterns, which indicated that silver was only homogenously distributed on the surface of the TiO$_2$ [32]. These results were consistent with the UV-Vis results where there was also no peak characteristic of silver around 450 nm detected [33]. The XRD patterns showed no peak which was not indexed or corresponding to silver oxide phase observed. This suggested that the nanocomposites prepared were of high purity. Increasing the concentration of silver on TiO$_2$ did not change the anatase phase. The average crystalline size of TiO$_2$ nanoparticles and Ag-TiO$_2$ nanocomposites was estimated using Debye-Scherrer formula.

$$D = k\lambda / (\beta COS\Theta) \qquad (6)$$

The average crystalline size of nanoparticles is denoted as (D), k is the geometric factor (0.9), λ is the wavelength of X-ray radiation source and β is the angular FWHM (full-width at half maximum) of the XRD peak at the diffraction angle Θ [36]. The crystallite sizes were 9.4 nm,

12.41 and 11.44 nm for Ag-TiO$_2$ (1 %) Ag-TiO$_2$ (3 %) and Ag-TiO$_2$ (5 %) respectively. There was no observable pattern which could be due to formation of clusters upon attachments of silver on the TiO$_2$ structure.

The (101) peak at a diffraction angle of 25,50^o was magnified to further observe the changes on the position of the peak as the amount of Ag was increased on TiO$_2$. Fig. 2 (b) shows that as the amount of Ag was increased from 1 % to 5 % the peaks became broader. This was attributed to Ag deposited on the surface of the TiO$_2$ crystal structure. It was also observed in Fig. 2 (b) that the (101) peak was slightly shifted to a lower diffraction angle. In the TiO$_2$ lattice, the Ti^{4+} is 68 Å and that of Ag is 126 Å, therefore for Ag$^+$ to replace the Ti^{4+}, high energy is needed and only a small amount of Ag$^+$ can enter the TiO$_2$ lattice to induce either O vacancies or deficiencies of Ti^{4+} 33. This is a further explanation why there was no visible peak in the Ag-TiO$_2$ nanocomposites [34, 35-37].
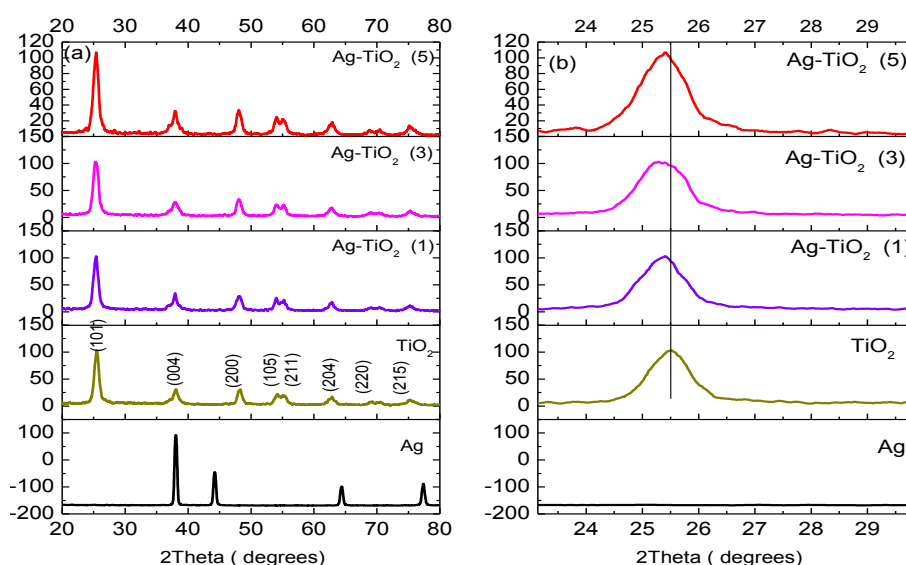
Fig. 2. (a) XRD patterns for Ag, TiO$_2$ and Ag- TiO$_2$ (1-5wt%) (a) and (b) the expanded position of (101) anatase peak in the XRD patterns for TiO$_2$ with respect to Ag-TiO$_2$ at different wt% of Ag (1-5 wt %).

The morphology and size of the nanoparticles and nanocomposites were further investigated through STEM analysis. Fig 3 (a-e) shows STEM images for Ag, TiO$_2$ and Ag- TiO$_2$ (1, 3, 5 wt %). The STEM image of Ag nanoparticles was observed to be predominately spherical. The mean particles size obtained from particle distribution curve (Gaussian fitting) was 21.54 ± 4.27 nm. The TiO$_2$ micrograph showed particles with non-uniform morphology and size but some agglomeration. The mean particle size was found to be 12.02 ± 3.85 nm. The non-uniform size could be attributed to the small amount of PVP, which might have not been enough hence inefficient in encapsulating particles into mono-dispersed shapes [38]. As the amount of silver was increased in the TiO$_2$ structure, the STEM images revealed the presence of silver appearing as bright white irregular shaped spots. The mean particle sizes were 6.78 ±1.44 nm, 10.64 ± 1.91 nm, 8.54 ± 2.01 nm for Ag-TiO$_2$ (1), Ag-TiO$_2$ (3) and Ag-TiO$_2$ (5) respectively. There was also no specific pattern in size as amount of Ag was increased on TiO$_2$ which was also evident with the XRD results and we attribute this to the un-uniform depositing of Ag on the TiO$_2$ [38].

Energy dispersive x-ray (EDX) analysis was performed to further establish the elemental presence and percentage weight of silver in the Ag-TiO$_2$ (1-5 wt %) nanocomposites and also to confirm the formation of individual Ag, and TiO$_2$. Fig. 3 (k- o) show the EDX spectra for Ag, TiO$_2$ and Ag-TiO$_2$ (1, 3 and 5 wt %). In the EDX spectra of TiO$_2$ (Fig. 3 (l) only Ti and O elements with no extra peaks of impurity were observed. However, in Ag-TiO$_2$ (1 wt%) (Fig.

3(m)) and Ag-TiO₂ (3 %) (Fig. 3 (n)) nanocomposites, minor traces of vanadium were observed. The Ag-TiO₂ (5 wt %) did not have any traces of vanadium impurity. This was attributed to impurities from STEM analysis. The assumption is based on the fact that there was no peak of impurity on the XRD patterns. The EDX data showed that the percentage weight for silver increased from 1.48, 4.33 to 7.75 %. This is in agreement with the STEM images which showed a gradual increase in silver appearing as white spots [39-40].
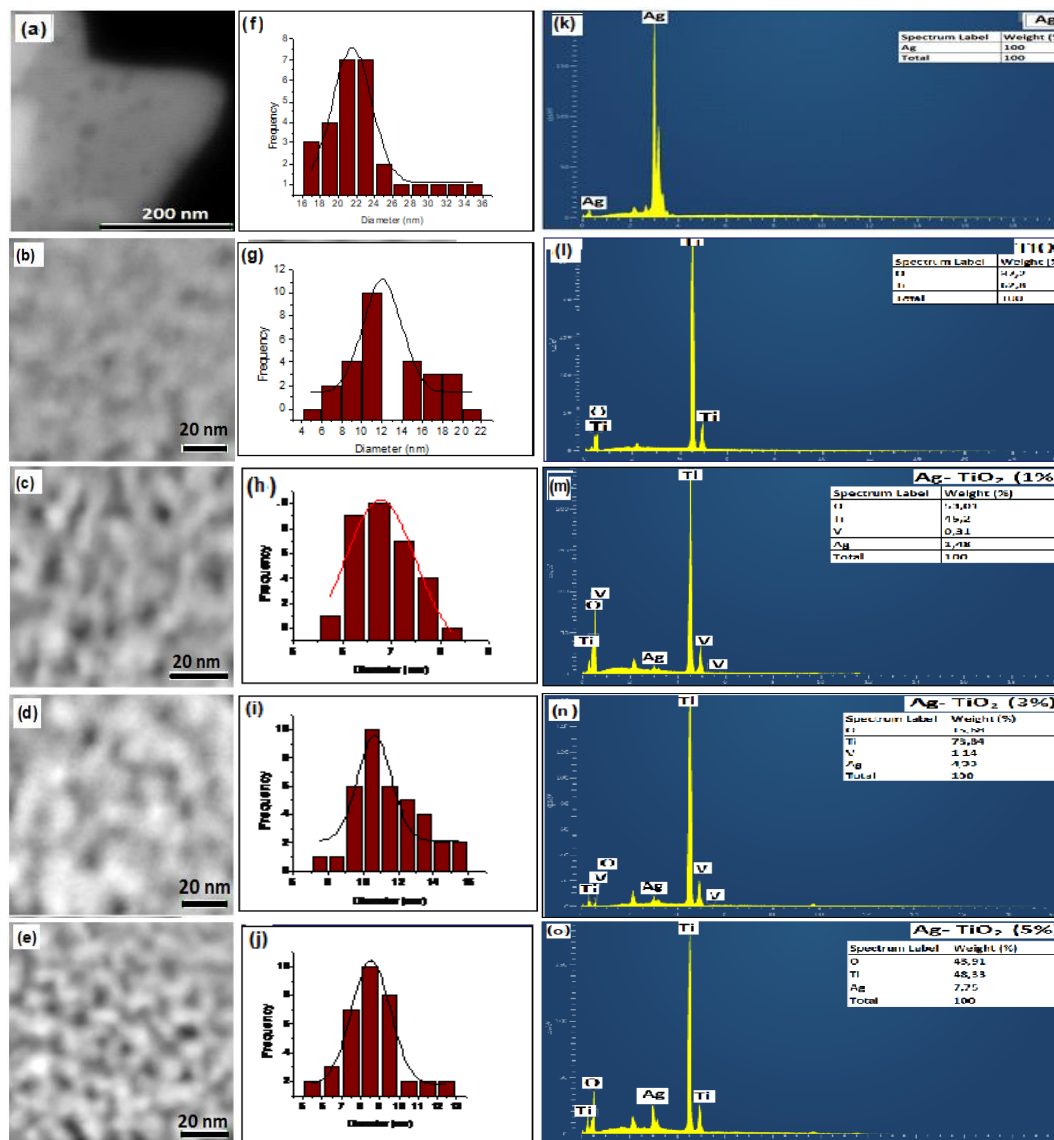
Fig. 3. STEM images (a-e), corresponding particles size distribution graphs (f –j) and energy dispersive X-ray (k-o) for Ag, TiO₂ nanoparticles and Ag-TiO₂ (1-5 wt%) nanocomposites.

The photocatalytic activity of nanoparticles (Ag, TiO₂ and Ag-TiO₂ (1, 3 and 5 wt %) on 2-chlorophenol, 2,4-dichlorophenol and 2,4,6-trichlorophenol was investigated under UV irradiation in aqueous medium. The degradation activity was carried out at initial concentrations of 25 ppm and 5 ppm of the chlorophenols. The nanocomposites that produced the highest degradation efficiency was further investigated at three pH values, 6.0, 8.0 and 11.0.

The results of photodegradation of 25 ppm 2- chlorophenol using Ag, TiO₂ and Ag-TiO₂ (1, 3, 5 wt%) catalysts indicated that within the first 20 minutes there was a rapid formation of other products. This was evidenced by the immediate appearance of two prominent absorbance peaks at 322 nm and 385 nm. The peak due to 2CP in the presence of catalyst was observed at 304

nm. Contrary to what is expected, the % degradation showed a steady increase in absorbance from 20 min to 100 min with a slight drop noticed after 100 min. It was therefore concluded that at 25 ppm, using the 16 W UV light photoreactor and the prepared nanoparticles/ nanocomposites, 2CP was immediately converted to intermediates which were not further mineralized within 120 min. The formation of intermediates with chlorophenols was also observed by Ba-Abbad et al. (2013) [41-42]. The intermediates that are mostly presence are catechol, hydroxyquinone and phenol [40]. However, no further investigation on the intermediates were done in the current study.

At 5 ppm 2-chlorophenol, there was also an appearance of new absorbance peak attributed to formation of intermediates at 377 nm. However, it was noticed that the peak was not as intense as it was at 25 ppm initial concentration of 2CP. Unlike at 25 ppm, an increase in the amount of 2CP was noticed within the first 20 minutes only. However, after 20 min there was a steady disappearance of the 2CP up to a total of 39.9 % degradation.

Photocatalytic degradation of 25 ppm 24DCP showed a sudden initial degradation drop of 5,7 %, 12.9 %, 10.8 %, 20.9 %, and 8.8 % within the first 20 min for Ag, TiO_2, Ag-TiO_2 (1), Ag-TiO_2 (3) and Ag-TiO_2 (5) respectively, after the introduction the UV light. The total degradation (120 min) for each catalyst improved to 6.7 %, 11.1 %, 15.6 %, 46.5 %, and 14.4 % for Ag, TiO_2, Ag-TiO_2 (1), Ag-TiO_2 (3) and Ag-TiO_2 (5) respectively. It was noted that the photocatalytic degradation was generally ineffective at this concentration, 25 ppm. There was some noted increase in the amount of the organic pollutant (24DCP) instead of it decreasing. The increase in the amount of 24DCP was also attributed to formation of intermediates [42, 43]. Fig. (b) shows the UV-Vis spectra of Ag-TiO_2 (3) which had the best % degradation (46.5 %) at this initial concentration, 25 ppm.

The results of photodegradation of 2,4-dichlorophenol at 5 ppm are shown in Fig. 4(a). The total % degradation was 16.9 %, 47.8 %, 52.8 %, 76.1 % and 60.0 % for Ag, TiO_2, Ag-TiO_2 (1), Ag-TiO_2 (3) and Ag-TiO_2 (5) respectively, with Ag showing still showing the list reduction. The results showed that % degradation was enhanced at 5ppm initial concentration of the pollutant. The results also indicate that addition of silver to TiO_2 improved the % degradation when compared to pure TiO_2 with Ag-TiO_2 (3) showing the highest reduction.

Photocatalytic degradation of 2,4,6-trichlorophenol at 25 ppm and 5 ppm initial concentrations using Ag, TiO_2 and Ag–TiO_2 (1,3,5 wt %) was also investigated. The results show that at 25 ppm with TiO_2, 22. 5% was degraded in the first 20 minutes and a total of 33.8 %. Silver nanoparticles showed a total of 17.0 % removal. As TiO_2 was loaded with Ag particles there was sudden % degradation, in the first 20 min of the organic pollutant amounting to 29.0%, 28.0% and 24.1 % for Ag-TiO_2 (1), Ag-TiO_2 (3) and Ag-TiO_2 (5), respectively. The formation of intermediates was noticed with 246TCP. Appearance of new absorbance peaks at 331 nm and 389 nm were observed [43].

At 5 ppm 2,4,6-trichlorophenol as shown in Fig. © there was an improved total degradation efficiency of 17,8 %, 20,0 4%, 59,8, 81,6, 87,9 % for Ag, TiO_2, Ag-TiO_2 (1), Ag-TiO_2 (3) and Ag-TiO_2 (5) respectively. Unlike at 25 ppm there was no observable new peak attributed to intermediates. The results are in agreement with those obtained with 2CP, 24DCP that Ag-TiO_2 (3) produced the best reduction of 246 TCP. Addition of Ag to TiO_2 produced better degradation efficiency of 246TCP compared to pure TiO_2. Patil, et al. (2014) made similar observations that lower initial concentration of the chlorophenols lead to an enhanced photocatalytic degradation efficiency [40].

To summarize, the results on initial concentration of the pollutant, it was observed that at 25ppm initial concentration of the organic pollutant, the photocatalytic degradation efficiency was low compared to when the concentration was 5 ppm. The explanation given was that at high concentration there are many organic molecules adsorbed to the surface of the catalyst but the available photo generated holes responsible for production of the hydroxyl radicals remain constant. This leads to limited hydroxyl radicals produced to attack all the organic molecules [44].
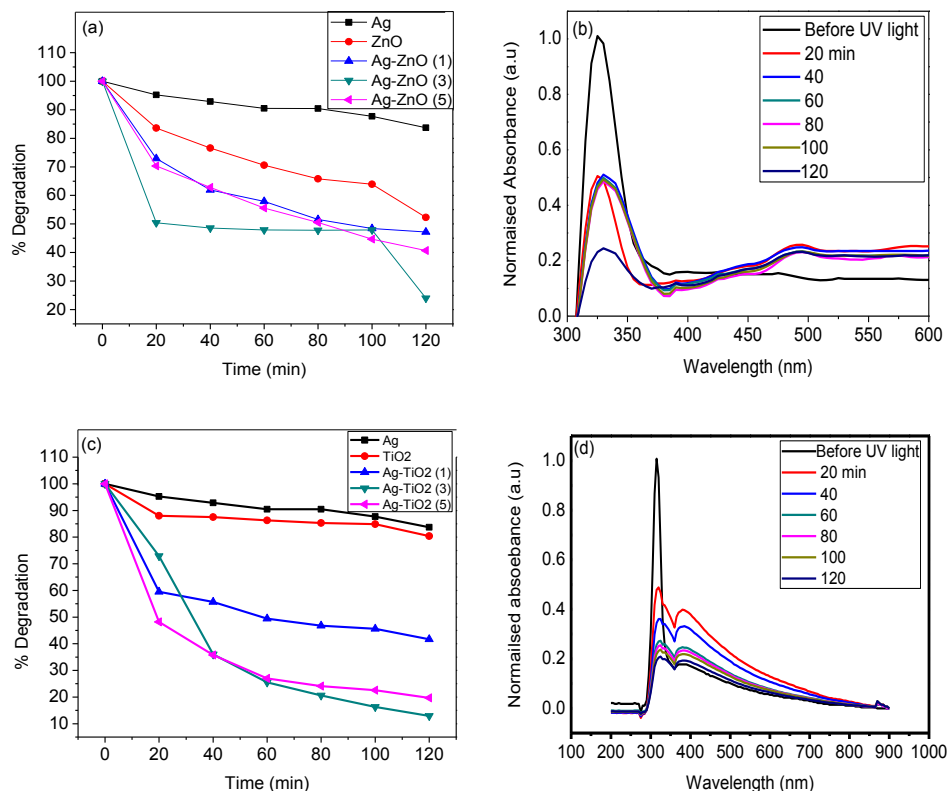
Fig. 4. (a) Photocatalytic degradation of 24DCP using Ag, TiO₂ Ag-TiO₂ (1, 3 and 5 wt %), (b) and corresponding UV –Vis spectrum using Ag-TiO₂ (3). (c) Photocatalytic degradation of 246TCP using Ag, TiO₂ Ag-TiO₂ (1, 3 and 5 wt %) and corresponding UV–Vis spectrum using Ag-TiO₂ (3). All chlorophenols are at 5 ppm concentration.

Photocatalytic degradation of 2CP was investigated at pH 4.0, 8.0 and 11.0. Fig. 5 (a and b) shows the results of photocatalytic degradation of 2CP at pH 11.0 using Ag-TiO₂ (3) nanocomposites as a catalyst. A total degradation of 39.9 % was obtained at pH 11.0, while pH 8.0 and 4.0, showed an increase instead of a decrease in the amount of the pollutant. This was attributed to the formation of intermediates as has already been indicated [36, 39]. Even though the % degradation efficiency at pH 11.0 was low (39.9 %), in comparison to pH 4.0 and 8.0 it can be concluded that degradation of 2CP was best at this pH 11.0.
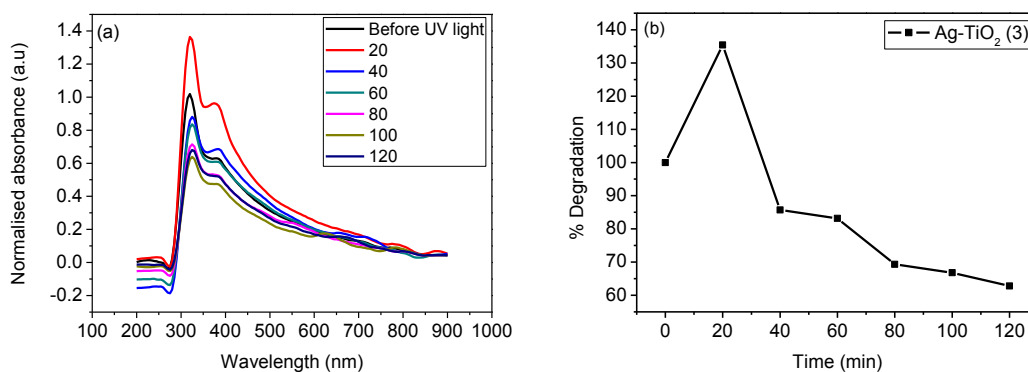
Fig. 5. UV-Vis spectrum (a) % degradation (b) showing photocatalytic degradation of 2-chlorophenol at 5 ppm and pH 11 using Ag-TiO₂ (3) at a catalyst concentration of 3.2 ppm.

Photocatalytic degradation of 24 DCP at pH 6.0, 8.0 and 11.0 showed a total degradation of 23.4 %, 60.0 % and 76.1 for pH 6.0, 8.0 and 11.0 respectively (Fig. 6). The results are in agreement with ones obtained for 2CP that a comparatively higher degradation was obtained at pH 11.

The pH plays an important role on photocatalytic activity because it affects the surface charge of the catalyst [41, 42, 45, 46]. In acidic medium (pH below the point zero charge for TiO_2, pH = 6.9, for 2CP) the surface of the TiO_2 is protonated and becomes positively charged. On the other hand, the TiO_2 surface is deprotonated in alkaline medium (above pH = 6.9). Equations 10 and 11 further illustrate the protonation and deprotonation of TiO_2 [45].

$$TiOH + H^+ \rightarrow TiOH_2^+ \qquad (7)$$

$$TiOH + OH^- \rightarrow TiO^- + H_2O \qquad (8)$$
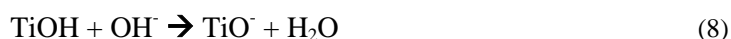
It follows that when the pH is increased the hydroxide ions become predominant. The presence of Ag, in the Ag-TiO_2 nanocomposites reduces the recombination rate hence the generated holes are more available to interact with hydroxide ions to produce the reactive hydroxyl radicals which are responsible for oxidizing the organic compounds as illustrated in the equation [40].

$$H_{VB}^+ + OH^- \rightarrow {}^{\cdot}OH \ (radical) \qquad (9)$$
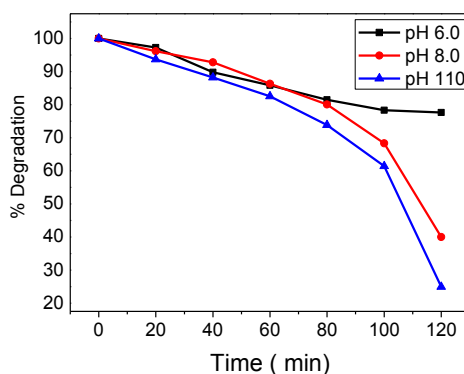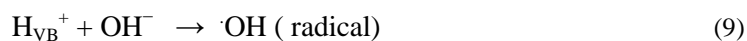
Fig. 6. Photocatalytic degradation of 24DCP at pH 6.0, 8.0 and 11.0.

4. Conclusions

Synthesis of Ag, TiO_2 and Ag-TiO_2 (1-5 wt %) were carried out by reduction and precipitation method for Ag and TiO_2, Ag-TiO_2 respectively. The UV-Vis of pure TiO_2 showed band gap of 3.38 eV. Addition of Ag to TiO_2 brought about a gradual decrease in band gap. However, the spectrum showed no observable peak for silver in the UV-Vis. The PL spectra was in agreement with the results of the UV-Vis as there was a decrease in intensity as the amount of silver was increased from 1,3 and 5 wt %. This was an indication that silver could cause a delay in the recombination rate of the excited electrons with the holes. The XRD patterns revealed an anatase structure of TiO_2.

It was revealed that addition of Ag to TiO_2 did not affect the anatase structure except a slight shift that was attributed to a small amount of Ag^+ entering the TiO_2 lattice inducing either O vacancies or deficiencies of Ti^{4+}. The XRD pattern confirmed the above statement in that there was no observable peak related to Ag. STEM results showed spherically shaped Ag nanoparticles and non- uniformly shaped TiO_2 and Ag-TiO_2. The photocatalytic degradation efficiency of pure

TiO$_2$ was lower compared to Ag-TiO$_2$. It was revealed photo catalytic degradation was enhanced at 5 ppm initial concentration of chlorophenols compared to 25 ppm. Degradation best efficiency of 39.9 % and 87.9 % of 2CP and 246 TCP was achieved at   pH 11.

Acknowledgements

References

[1] M. Ouzzine, J. A. Maciá-Agulló, M. A. Lillo-Ródenas, C. Quijada, A. Linares-Solano, Appl. Catal. B Environ. **154,** 285 (2014).

[2] R. Chauhan, A. Kumar, R. P. Chaudhary, Res. Chem. Intermed **4,** 1443 (2014).

[3] B. Rajamannan, S. Mugundan, G. Viruthagiri, N. Shanmugam, P. Praveen, Int. J. Current Res. **5**, 2863 (2013).

[4] M. I. Dar, A. K. Chandiran, M. Gr¨atzel, M. K. Nazeeruddin, S. A. Shivashankar, J. Mater. Chem. B **2**, 1662 (2014).

[5] M. Quzzine, M. A. Lillo-Rodenas, A. Linares-Solano, Appl. Catal. B **134**, 333 (2013).

[6] D. S. Sharmila, R. Venckatesh, S. Rajeshwari, Int. J. Innovative Res. Sci. Eng. Technol. **3**, 15206 (2014).

[7] M. K. Seery, R. George, P. Floris, P. S. C. Pillai, S. J. Photochem. Photobiol. A: Chem. **189**, 258 (2007).

[8] M. A. Behnajady, N., Modirshahla, R. Hamzavi, J. Hazard. Mater. B **133**, 226 (2005).

[9] N. Bahadur, K. Jai, A. Srivastava, G. R. Govind, D. Haranath, M. S. Dulat, Chem. Phys. Mater. **124**, 600 (2010).

[10] M. Guzman, G. J. S. Dille, Nanomed. Nanotech. Biol. Med. **8**, 37 (2011).

[11] K. Gupta, R. P. Singh, A. Pandey, A. Pandey, J. Nanotechnol. **4**, 345 (2013).

[12] Y. Zheng, C. Chen, Y. Zhan., X. Lin, Q Zheng, K. Wei, J. Zhu, J. Phys. Chem. **112**, 10773 (2008).

[13] C. Karunakaran, V. Rajeswari, P. Gomathisankar, Solid State Sci. **13**, 923 (2011).

[14] J. Morales, A. Maldonado, A. M. de la, L. Olvera, 10th Int. Conf. Electr. Engineer. Comput. Sci. Auto. Control (CCE) Mexico City, Mexico. 2013.

[15] M. M. Byranvanda, M. H. Bazarganb, A. N. Kharata, **1109**, 111 (2012).

[16] M. M. Karkare, Int. Nano Lett. **4**,111 (2014).

[17] M. U. Rashid, M. Bhuiyan, H. Khairul, M. E. Quayum, J. Pharmaceutical Sci. **12**, 29 (2013).

[18] J. Bai, Y. Li, J. Du, S. Wang, J. Zheng, Q Yang, X. Chen, Mater. Chem. Phys. **106,** 412 (2007).

[19] T. H. Tran, D. C. Ta, D., V. T. Nguyen, Nanotechnology Article ID 497873 (2013).

[20] S. Alabbad, S. F. Adil, M. E. Assal, M. Khan, A. Alwarthan, M. R. H. Siddiqui, Arabian J. Chem. **7**, 1192 (2014).

[21] M. Stollera, M. Mescia, C. V. Peroni, A. Chianese, Chem Eng Trans **11**, 71.

[22] K. Mavani, M. Shah, Inter. J. Engineer. Res. Technol. **2,** 1 (2013).

[23] P. Manikandan, P. N. Palanisamy, R. Ramya, D. Nalini, Inter. J. Emerg. Technol. Comput. Appl. Sci. **9**, 148 (2014).

[24] B. Otieno, S. Apollo, B. Naidoo, A. Ochieng, Proceedings of ISERD International Conference. Jerusalem, Israel, 29th - 30th December 2016.

[25] L. Peiqiang, H. Haitao, X. Jinfeng, J. JHua, P. Hui, L. Jing, W. Chenxiao, A. Shiyun, Appl. Catal. B: Environ. **147**, 912 (2014).

[26] S. Kuriakose, V. Choudhary, B. Satpati, S. Mohapatra, Beilstein J Nanotechnol **5,** 639 (2014).

[27] Z. L. Wang, Mater. Today. **7**, 26 (2004).

[28] W. Xie, Y. Li, W. Sun, J. H. Huang, H. Xie, X. Zhao, J. Photochem. Photobio. A: Chem. **216**, 149 (2010).

[29] J. Liqiang, Q. Yichun, W. Baiqi, L. Shudan, J. Baojiang, Y. Libin, F. Wei, F. Honggang, S.

Jiazhong, Sol. Energ. Mat. Sol. Cells **90**, 1773 (2006).

[30] K. Jyoti, M. Baunthiyal, A. Singh, J Radiat Res Appl Sci **9**, 217 (2016).

[31] M. Sahu, B. Wu, L. Zhu, C. Jacobson, W. N. Wang, K. Jones, Y. Goyal, Y. J. Tang, P. Biswas, Nanotechnol. **22**, 41 (2012).

[32] A. K. A. Gafoor, M. M. Musthafa, P. P. Pradyumnan, Nanoparticles. J. Electronic. Mater. **41**, 2387 (2012).

[33] A. Ashkarran, J. Theor. Appl. Phys. **4**, 1 (2011).

[34] S. Talam, S. R. Karumuri, N. Gunnam, **2012**, Article ID 372505 (2012).

[35] S. X. Liu, J. T. Kim, Membrane J. Adhes Sci. Technol. **25**, 1 (2011).

[36] T. D. Pham, B. K. Lee, Int. J. Environ. Res. Public. Health. **11**, 3271 (2014).

[37] P. Navabpour, K. Cooke, H. Sun, Coatings **7**, 10 (2017).

[38] H. M. Kamari, M. G. Naseri, E. B. Saion, Metals **4**, 118-129.

[39] M. M. Ba-Abbad, A. A. H. Kadhum, A. B. Mohamad, M. S. Takriff, K. Sopian, K. Res. Chem. Intermediat **39**, 1981 (2013).

[40] S. Ahmed, M. G. Rasul, W. N. Martens, R. J. Brown, M. A. Hashib, Desalination **261**, 3 (2010).

[41] F. C. S. Paschoalino, M. P. Paschoalino, E. Jordão, W. F. Jardim, (2012) Open J. Phys. Chem. **2**(3), Article ID: 22095, 6 pages (2012).

[42] S. S. Patil, S. T. Patil, S. P. Kamble, Inter. J. Engineer. Sci. **3**, 38 (2014).

[43] A. Gnanaprakasam, V. M. Sivakumar, M. Thirumarimurugan, Indian J. Mater Sci. **2015** Article ID 601827, 16 pages (2015).

[44] N. C. Tolosa, M. C. Lu, H. D. Mendoza, A. P. Rollon, Sustain. Environ. Res. **21**(6), 381 (2012).

[45] T. Singh, N. Srivastava, P. K. I. Mishra, A. K. Bhatiya, N. Lal Singh, Mater. Sci. Forum **855**, 20 (2016).